CrystEngComm

ROYAL SOCIETY OF CHEMISTRY

PAPER

View Article Online
View Journal | View Issue

Cite this: *CrystEngComm*, 2026, **28**, 169

Size-controlled synthesis of monodisperse zinc gallium oxide particles *via* coprecipitation under hydrothermal conditions using trisodium citrate

Fumiyuki Shiba, * Naoki Koyama and Yusuke Okawa

Received 2nd October 2025,
Accepted 16th November 2025

DOI: 10.1039/d5ce00952a

rsc.li/crystengcomm

Monodisperse particles of zinc gallium oxide have been synthesized *via* coprecipitation under hydrothermal conditions in the presence of trisodium citrate, which acts as a ligand for the reactant metal ions to establish controlled homogeneous nucleation at an elevated temperature. This procedure enables the particle size to be tuned up to about 200 nm by changing the citrate concentration. Also, the spinel crystal structure can be maintained when the compositional ratio of Ga to Zn in the particle, $f_{Ga/Zn}$, varies, at least in the range of $f_{Ga/Zn}$ = 1.3–2.7, depending on the citrate concentration and/or Ga^{3+}/Zn^{2+} ratio in the reacting solution. The absorption edge of the diffuse reflectance spectra suggests that the present particles possess a band gap of 4.7–4.9 eV, which is almost independent of the synthesis conditions.

Introduction

Particulate materials are one of the important categories of functional materials. Each particle will act as an independent unit of the functionality, and its properties often depend on its size due to its large specific area. Thus, monodisperse particles, which have a very narrow distribution of size, may be one of the ideal forms ensuring the functionality of particulate materials.[1] The typical strategy for the synthesis of monodisperse particles is to make the growth history of all the particles the same by separating the short nucleation period from the following growth period, which is known as the LaMer mechanism.[2] However, implementing this concept depends on the chemical reactions involved in the synthesis of the target substances. Hence, studies on designing and optimizing the reaction procedure are still essential to obtain monodisperse particles of various substances.

Zinc gallium oxide (ZGO; zinc gallate), the target substance in this study, is a gallium compound that has a normal spinel structure, where Zn^{2+} and Ga^{3+} ions are located at the tetrahedral and octahedral positions, respectively (space group $Fd\bar{3}m$).[3,4] Although its stoichiometric formula is $ZnGa_2O_4$, the atomic ratio of Ga to Zn in ZGO, $f_{Ga/Zn}$, can be varied, while keeping its spinel structure.[5]

ZGO is a wide-bandgap semiconducting material ($E_g \sim 5$ eV)[6] applied in electronic devices.[7–10] ZGO is also expected to be a light-emitting material, typically by doping activating ions such as Mn^{2+} ions[11–13] or lanthanide ions.[14,15] Also, Cr^{3+} and Gd^{3+} ions are especially interesting due to their persistent luminescence property, which is useful for *in vivo* imaging.[4,16–21] In addition, two or three types of ions are sometimes co-doped to enhance the functionality of the emitted light.[22–27] Another application of ZGO is as a photocatalyst, which has been widely studied for splitting water,[28,29] reducing CO_2,[30–32] degrading organic compounds,[33–37] *etc.*

There are various reports on the synthesis of ZGO, including physical and chemical methods. The former includes RF sputtering,[10] chemical vapor deposition,[6,9,38] and pulse laser deposition.[13] These procedures enable the production of a thin film structure on a substrate under dry conditions suitable for the fabrication of electronic devices.

In the case of the latter, one of the typical procedures is the solid-phase reaction, in which ZnO and Ga_2O_3 powders are mixed and heated at *ca.* 1000 °C to form the ZGO phase.[4,7,12,16,39] In this method, $ZnGa_2O_4$ may be formed by mixing the raw materials in a stoichiometric ratio. However, sufficient mixing, grinding, and pressing, in addition to high temperature, are essential for the reaction to progress efficiently at an adequate reaction rate.

The calcination of various precursors is also often employed to obtain ZGO solids at lower temperatures than the solid-phase reaction. Gel-like hydroxides formed by adding NH_3 to the metal ion solution are typical of the precursor.[23,33] Layered double hydroxides (LDH)[40] and polyethylene oxide xerogels[32] are other types of precursors applied. Duan *et al.*[41] employed citric acid to form precursor

Department of Materials Science, Chiba University, 1-33 Yayoicho, Inageku, Chiba 263-8522, Japan. E-mail: shiba@faculty.chiba-u.jp

gels in the aqueous phase. Li *et al.*[36] utilized metal–acetylacetonate complexes in a homogeneous ethanol solution.

Liquid-phase processes in hydrothermal synthesis are applicable to obtain particulate forms of ZGO based on the following reaction:

$$Zn^{2+} + 2Ga^{3+} + 8OH^- \rightarrow ZnGa_2O_4 + 4H_2O \quad (1)$$

In this way, nano-sized ZGO particles, smaller than 20 nm, are usually formed in the typical reaction pH range of 9–11, adjusted with NH_3 (ref. 15, 18, 24, 25, 28, 34 and 42–44) or urea.[14,21,45] Some additives assist in increasing the size and/or regulating the shape of the formed ZGO particles. For example, sodium oleate[29] and ethylenediamine[46] act as growth modifiers to form thin platelet ZGO particles. The use of citric acid (or sodium citrate) is also effective for achieving morphology control. For example, Zhang *et al.* reported the preparation of hollow spherical ZGO particles with citric acid under acidic conditions.[31] Monodisperse spherical ZGO particles were obtained under basic conditions using trisodium citrate.[17,19]

Given that a series of different-sized monodisperse particles enables us to evaluate their size-dependent properties, including size independence, it is desirable to establish synthesis procedures that generate monodisperse particles with systematically controlled sizes of the target materials. The control of the metal ion composition is also essential if the target multi-metal oxide allows non-stoichiometric compositions. In this sense, the contribution of citrate ions to the formation of ZGO particles is a worthwhile area of study. However, the precise effect of citrate ions has not been demonstrated in a hydrothermal system for the synthesis of monodisperse ZGO particles, despite the effect of the dopant Co^{2+} ions as a size controller.[19] Moreover, the influence of citrate ions on the composition of ZGO has not been evaluated, despite their ability to form complexes with Zn^{2+} and Ga^{3+} ions.

Thus, in this study, we propose a procedure for the synthesis of monodisperse spherical ZGO particles using trisodium citrate under hydrothermal conditions, allowing the systematic variation of their particle size and Ga/Zn ratio. The role of citrate ions in the formation process is discussed. Also, the band-gap energy and the fluorescence spectra of the present particles are evaluated.

Experimental

Materials

The chemicals used are $Zn(NO_3)_2{\cdot}6H_2O$ (99.9%), $Ga(NO_3)_3{\cdot}nH_2O$ (99.9%), trisodium citrate dihydrate (GR), and NaOH (1 mol L^{-1}, for volumetric titration), which were purchased from FUJIFILM Wako Pure Chemicals, Japan, and used without further purification.

Hydrothermal synthesis of ZGO particles

The procedure for the synthesis of the ZGO particles in the present study was typically as follows. Distilled water (8.5 mL), 0.1 mol L^{-1} $Zn(NO_3)_2$ aqueous solution (2.5 mL), and 0.1 mol L^{-1} $Ga(NO_3)_3$ aqueous solution (5 mL) were mixed in a glass vessel and placed in a water bath at 40 °C. Then, under magnetic stirring, 0.25 mol L^{-1} trisodium citrate (Na_3-Cit) aqueous solution (4 mL) and 0.42 mol L^{-1} NaOH aqueous solution (5 mL) were introduced into it in that order. After being kept at 40 °C for 60 min with stirring, the mixed solution was transferred to a Teflon-lined autoclave and placed in an air oven at 150 °C for 24 h. The formed precipitate was separated from the aqueous phase by centrifuging at 10 000 rpm for 15 min. After removing the supernatant solution, the precipitate was redispersed in distilled water and centrifuged; this process was repeated once more. Then, the precipitate was freeze-dried.

The reactant concentrations after mixing correspond to C_{Zn} = 10 mmol L^{-1}, C_{Ga} = 20 mmol L^{-1}, C_{cit} = 40 mmol L^{-1}, and C_{NaOH} = 84 mmol L^{-1} for $Zn(NO_3)_2$, $Ga(NO_3)_3$, Na_3-Cit, and NaOH, respectively, under the typical conditions. In the case of varying the C_{Ga}/C_{Zn} ratio, the total concentration of the metal ions was kept constant as $C_{Zn} + C_{Ga}$ = 30 mmol L^{-1}; $C_{NaOH} = 1.05 \times (2C_{Zn} + 3C_{Ga})$ as equivalent to 5% excess to the stoichiometric formation of $Zn(OH)_2$ and $Ga(OH)_3$. Also, the total volume was set to 25 mL in all conditions by changing the volume of distilled water when C_{cit} and/or C_{NaOH} were varied.

Characterization

The size and shape of the particles were evaluated *via* TEM (Hitachi H-7650, operated at 100 kV) and FE-SEM (JEOL JSM-6700F, operated at 15 kV; the specimens were coated with Pt). Their crystal structure was identified by powder XRD analysis using a Bruker D8 Advance (Cu Kα, λ = 1.5418 Å).

Atomic absorption spectrometry (AAS) was employed to estimate the elemental composition of the particles by determining the Zn^{2+} and Ga^{3+} ions remaining in the supernatant solution after the hydrothermal reaction. The supernatant solution (4 mL) was diluted to 20 mL, which also contained HNO_3 at 0.3 mol L^{-1}, to apply AAS measurement using an air/acetylene flame with a Varian SpectrAA55 at absorption lines of λ = 213.9 nm and 294.4 nm for Zn and Ga, respectively. TEM-EDX measurement was also applied to the ZGO particles to ensure the AAS determination of their composition.

To estimate the band-gap energy, E_g, a Shimadzu UV-3100PC spectrophotometer with an integral sphere was used to obtain the diffuse reflectance spectra of the ZGO particles dispersed in $BaSO_4$ as the matrix at 1 wt%. Photoluminescent spectra were measured using a JASCO FP-8300 fluorescence spectrometer.

Results and discussion

Formation of monodisperse ZGO particles with Na_3-Cit

Fig. 1 shows the TEM and FE-SEM images of the ZGO particles hydrothermally synthesized at C_{Ga}/C_{Zn} = 2 (150 °C, 24 h) in the absence and presence of Na_3-Cit. Under the former condition (*i.e.*, C_{cit} = 0 mmol L^{-1}), the precipitate is in the form of nanoparticles having mean diameter (D) ± one standard deviation (σ) = 9.5 nm ± 2.1 nm (Fig. 1a and b). Conversely, under the latter condition (C_{cit} = 40 mmol L^{-1}), monodisperse spherical particles with $D \pm \sigma$ = 209 nm ± 20 nm are obtained (Fig. 1c and d; the coefficient of variation, COV, is 9.6%), indicating the effectiveness of Na_3-Cit in increasing the size of the ZGO particles. In addition, the relative size distribution is narrower in the presence of Na_3-Cit, improving the monodispersity.

Fig. 2 indicates the XRD patterns of the ZGO particles shown in Fig. 1. The peaks are located at the same diffraction angles in both patterns and match with that of $ZnGa_2O_4$ with a spinel structure (ICDD PDF 01-071-0843). Meanwhile, the peak widths are different, reflecting their particle sizes, implying that the crystallite size increases with the growth of the particles in the presence of Na_3-Cit. In fact, the continuous lattice pattern in the HR-TEM image in Fig. S1 in the SI suggests the single crystalline structure of the ZGO particles. According to the diffraction angle, 2θ = 35.56°, of the strongest peak for the 311 reflection in Fig. 2b, the lattice parameter for the spinel cubic cell is estimated as a = 8.37 Å, which is in good agreement with the literature (a = 8.33 Å).[3]

The presence of Na_3-Cit affects the composition and the yield of the particles. The AAS measurement indicated that virtually all the Zn^{2+} ions were converted to the solid phase from the aqueous solution, irrespective of the C_{cit} conditions. Conversely, 5.1% and 22.4% of unreacted Ga^{3+} ions were

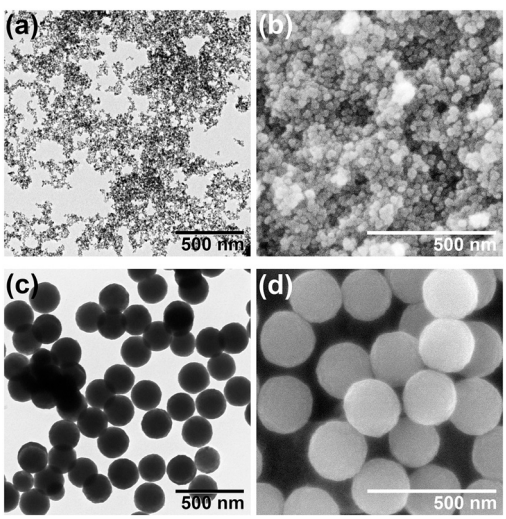

Fig. 1 TEM (the left column) and FE-SEM (the right column) images of the ZGO particles prepared in the (a) and (b) absence and (c) and (d) presence (40 mmol L^{-1}) of Na_3-Cit at C_{Ga}/C_{Zn} = 2 under the hydrothermal conditions at 150 °C for 24 h.

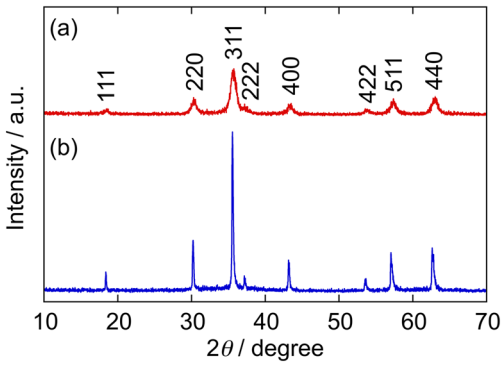

Fig. 2 XRD patterns of the precipitates shown in Fig. 1 (C_{Ga}/C_{Zn} = 2) obtained at C_{cit} = (a) 0 and (b) 40 mmol L^{-1} (Cu Kα radiation, λ = 1.5418 Å). The peaks are consistent with those for $ZnGa_2O_4$ (ICDD PDF 01-071-0843).

detected in the supernatant solution for C_{cit} = 0 and 40 mmol L^{-1} after 24 h reaction at 150 °C, giving non-stoichiometric compositions of the ZGO particles as $ZnGa_{1.90}O_{3.85}$ and $ZnGa_{1.55}O_{3.33}$, respectively, due to the reaction condition of C_{Ga}/C_{Zn} = 2 for these particles. The Ga/Zn atomic ratios in the particles, $f_{Ga/Zn}$, were also confirmed by TEM-EDX analysis; the estimated compositions by TEM-EDX were in good agreement with that obtained from AAS (Fig. S2 in SI). Thus, the yield, y, was calculated to be y = 96.7% and 85.0% for C_{cit} = 0 and 40 mmol L^{-1}, respectively, by defining y as follows:

$$y = (x_{Zn}C_{Zn} + x_{Ga}C_{Ga})/(C_{Zn} + C_{Ga}) \quad (2)$$

where x_{Zn} and x_{Ga} are the conversion percentages for Zn^{2+} and Ga^{3+} ions, respectively.

Na_3-Cit also affects the behavior of the reacting solution before hydrothermal treatment is applied. In the absence of Na_3-Cit, white precipitates were immediately formed upon introducing the NaOH solution into the solution of metal ions. According to the AAS measurement, it was estimated that at this stage, 99.9% of Zn^{2+} ions and 66.6% of Ga^{3+} ions coprecipitated from the solution phase containing them at C_{Zn} = 10 mmol L^{-1} and C_{Ga} = 20 mmol L^{-1}, respectively. Although the XRD pattern (Fig. S3 in SI) suggests that the white precipitate contains the Zn/Ga-LDH phase,[40,47] an amorphous hydroxide phase might also exist, given that the Ga^{3+} content, $f_{Ga/Zn}$ = 1.33, seems to be much higher compared to that expected from general LDHs (typically $f_{M^{3+}/M^{2+}}$ = 0.2 − 0.5).[48,49]

On the contrary, for C_{cit} = 40 mmol L^{-1}, the mixed solution remained transparent even after the addition of NaOH due to the formation of complex species that lower the free Zn^{2+} ion concentration, preventing coprecipitation before the temperature was elevated to hydrothermal conditions. Although both Zn^{2+} and Ga^{3+} ions are amphoteric, the solubilities of their hydroxides are quite different around the reaction pH range (pH 9.0 ± 0.5; including the conditions below). The solubilities of $Zn(OH)_2$ and $Ga(OH)_3$ can be

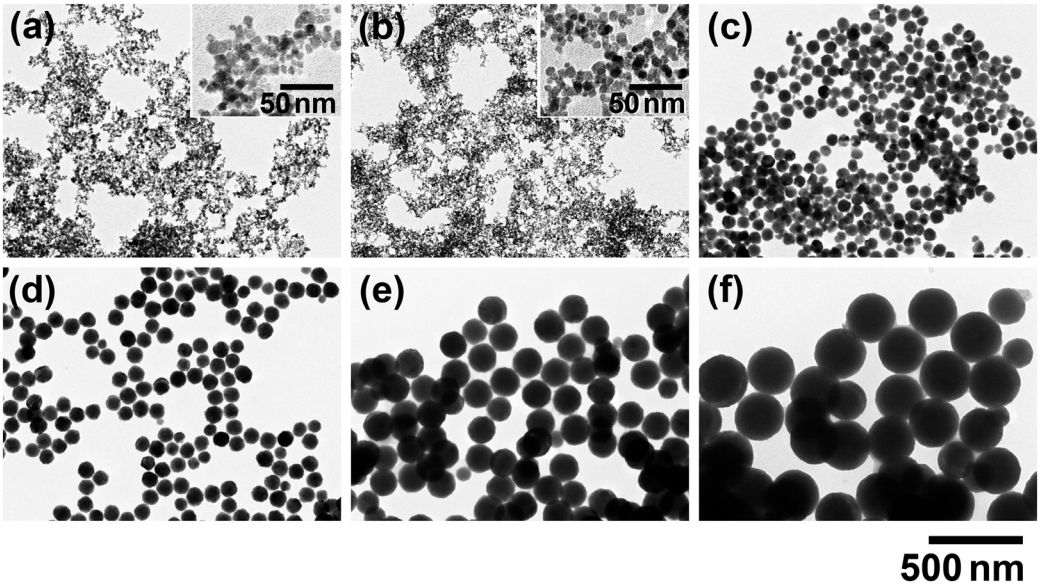

Fig. 3 TEM images of the ZGO particles synthesized under different C_{cit} conditions at (a) 0 mmol L^{-1}, (b) 15 mmol L^{-1}, (c) 25 mmol L^{-1}, (d) 30 mmol L^{-1}, (e) 40 mmol L^{-1}, and (f) 60 mmol L^{-1} at C_{Ga}/C_{Zn} = 2.57 (C_{Zn} + C_{Ga} = 30 mmol L^{-1}) and 150 °C for 24 h. The higher magnification images for (a) and (b) are also indicated in the insets.

estimated to be 1.5 × 10^{-6} mol L^{-1} and 4.0 × 10^{-2} mol L^{-1}, respectively, at pH 9.0 from the equilibrium constants at room temperature (Fig. S4 in SI).[50] Therefore, the central role of Na_3-Cit is as a complexing agent for Zn^{2+} ions[51] to achieve controlled precipitation from the homogeneous solution phase at the hydrothermal temperature.

Reflecting the role of Na_3-Cit, the addition order of the reactant solutions was critical, where even in the presence of Na_3-Cit, tiny ZGO particles, similar to that in Fig. 1a, were formed if the NaOH solution was added prior to the Na_3-Cit solution. In this case, the white precipitate remained even after the introduction of Na_3-Cit; Na_3-Cit did not dissolve the white precipitate effectively once it had formed. This result supports the importance of homogeneous nucleation at the hydrothermal temperature for monodisperse ZGO particles.

Here, it should be noted that no precipitate was formed by hydrothermal treatment in the absence of Zn^{2+} ions, owing to the low free Ga^{3+} ion concentration due to the formation of a complex with citrate ions,[52] in addition to $[Ga(OH)_4]^-$.[50] Thus, the present system may be classified as a coprecipitation process, triggered by the release of Zn^{2+} ions.

Effect of Na_3-Cit concentration

To evaluate the effect of Na_3-Cit more precisely, ZGO particles were synthesized under various C_{cit} conditions in the same manner at 150 °C for 24 h, where C_{Ga}/C_{Zn} = 2.57 to increase the $f_{Ga/Zn}$ ratio to around the stoichiometric value. The TEM images of the ZGO particles are indicated in Fig. 3; the histogram of the particle size for each C_{cit} condition is shown in Fig. S5 in the SI; the values of D, σ, and COV are listed in Table S1 in SI. Also, Fig. 4 shows the dependence of D and $f_{Ga/Zn}$ on C_{cit}. In the region at C_{cit} ≥ 25 mmol L^{-1}, the size of the ZGO particles increased up to $D \pm \sigma$ = 240 nm ± 23 nm at C_{cit} = 60 mmol L^{-1}, depending on C_{cit}. The particle shape seems spherical under each C_{cit} condition, although the particles tend to coagulate when C_{cit} exceeds 60 mmol L^{-1}.

On the contrary, there seems to be no contribution from Na_3-Cit to the particle size at C_{cit} = 15 mmol L^{-1}; the particles (Fig. 3b) are almost the same as that at C_{cit} = 0 mmol L^{-1} (Fig. 3a). This should result in the formation of white precipitate upon the addition of NaOH due to the insufficient complex formation with Zn^{2+}. In contrast, at C_{cit} ≥ 25 mmol L^{-1}, the reacting solutions maintained their transparent state until being transferred to the autoclave, indicating that it is important to maintain the homogenous solution state until

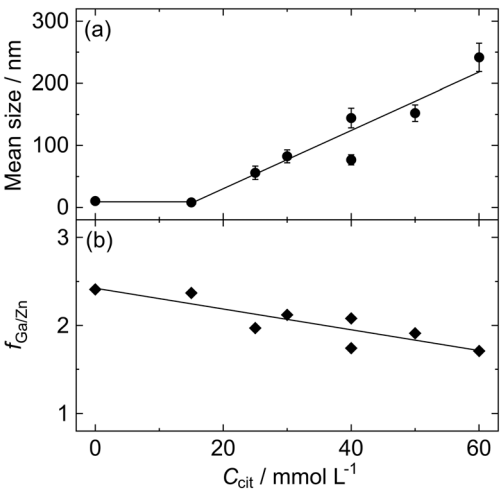

Fig. 4 Effect of the Na_3-Cit concentration (C_{cit}) on (a) the mean size and (b) atomic Ga/Zn ratio ($f_{Ga/Zn}$) of the ZGO particles synthesized under the conditions at C_{Ga}/C_{Zn} = 2.57 and 150 °C for 24 h.

elevating the temperature to ensure the effectiveness of Na_3-Cit for the controlled synthesis of ZGO particles. However, reflecting the complex formation property, the $f_{Ga/Zn}$ value decreased from 2.41 at C_{cit} = 0 mmol L^{-1} to 1.71 at C_{cit} = 60 mmol L^{-1} (Fig. 4b).

The size of monodisperse particles reflects the number of particles formed from the point of view of the mass-balance relationship. This means that a larger particle size corresponds to a smaller number of spontaneous nuclei. According to the spontaneous nucleation model for monodisperse particles, the number of formed particles, n, is expected to be proportional to the supply rate of the reactant species, Q_o, and inversely proportional to the volume increase rate, $\dot{v}$, during the nucleation stage as follows:

$$n = Q_o V_m / \dot{v} \quad (3)$$

where V_m is the molar volume of particles.[53] This equation implies that the number of nuclei decreases under the conditions of lower Q_o and/or faster $\dot{v}$. In the present case, the former may be more critical. That is, a higher C_{cit} would make the complexes more stable, inhibiting the release of the Zn^{2+} and Ga^{3+} ions. On the contrary, it seems that there is no reason for the increased intrinsic growth rate of ZGO particles in the presence of citrate ions; instead, citrate ions could reduce the growth rate if they adsorb onto the particle surface.

Precisely, this equation requires a consistent yield among the conditions for a quantitative discussion, and the present results do not meet this requirement; y = 95.5% at C_{cit} = 0 mmol L^{-1}, whereas y = 75.9% at C_{cit} = 60 mmol L^{-1}, reflecting a decrease in $f_{Ga/Zn}$ with an increase in C_{cit}, despite the almost 100% conversion for Zn^{2+}. However, the size control mechanism cannot be explained in terms of the yield difference, given that larger ZGO particles are formed under lower yield conditions, as indicated in Fig. 4. Thus, the discussion on eqn (3) has a certain validity at least qualitatively.

Effect of Ga/Zn ratio in the reacting solution

To evaluate the effect of the Ga/Zn ratio in the reacting solution, ZGO particles were synthesized under various C_{Ga}/C_{Zn} conditions (C_{Ga}/C_{Zn} = 1.59–3.41, $C_{Zn} + C_{Ga}$ = 30 mmol L^{-1}) at C_{cit} = 0 mmol L^{-1} and 40 mmol L^{-1}. The spinel ZGO phase precipitated under all the tested conditions.

Fig. 5 indicates the particle size, D, and the Ga/Zn ratio in the ZGO particles, $f_{Ga/Zn}$, as a function of C_{Ga}/C_{Zn}. In the absence of Na_3-Cit, the C_{Ga}/C_{Zn} ratio does not contribute to altering D (= *ca.* 10 nm) by reflecting the formation of a white precipitate before the hydrothermal treatment, similar to the above-mentioned cases. Alternatively, in the presence of Na_3-Cit, an increase in C_{Ga}/C_{Zn} (*i.e.*, higher C_{Ga} and lower C_{Zn}) results in a smaller D (*i.e.*, larger n). This result supports that the free Zn^{2+} ion concentration is the determining parameter for D, according to the comparison of the tendency in Fig. 3 and 4a, in which a smaller D tends to decrease under lower C_{cit} conditions, which gives a relatively higher concentration of free Zn^{2+} and Ga^{3+} ions.

On the contrary, $f_{Ga/Zn}$ proportionally depends on C_{Ga}/C_{Zn} under both C_{cit} conditions with different slopes, as shown in Fig. 5b. The slopes of 0.94 and 0.75 for C_{cit} = 0 mmol L^{-1} and 40 mmol L^{-1} imply about 6% and 25% of Ga^{3+} ions remain in the supernatant phase, irrespective of C_{Ga}/C_{Zn}, under the respective C_{cit} conditions after the reaction, respectively. As discussed above, this conversion inefficiency of Ga^{3+} would be due to the larger stability constants of its complexes.

Although the spinel structure was maintained within the C_{Ga}/C_{Zn} range (Fig. S6 in SI), the lattice parameter for its cubic cell, a, slightly differs among the particles depending on the $f_{Ga/Zn}$ value. As shown in Fig. 6, the value of a, estimated from the diffraction angle for the 311 reflection, linearly decreases with $f_{Ga/Zn}$ but is independent of the Na_3-Cit condition. This result seems to be reasonable given that

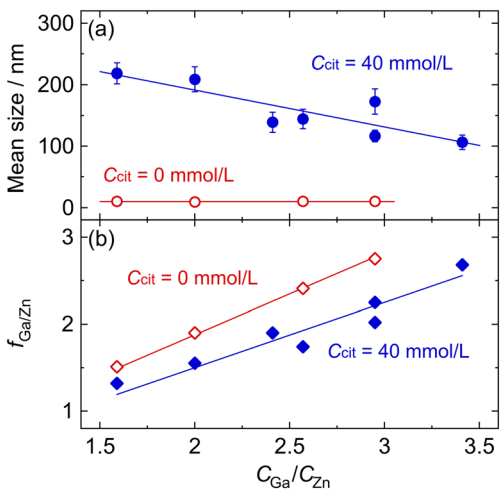

Fig. 5 Effect of the $Ga(NO_3)_3/Zn(NO_3)_2$ ratio contained in the reacting solution, C_{Ga}/C_{Zn}, on (a) the mean size and (b) the Ga/Zn atomic ratio in the particles, $f_{Ga/Zn}$, in the absence and presence (C_{cit} = 40 mmol L^{-1}) of Na_3-Cit (150 °C and 24 h).

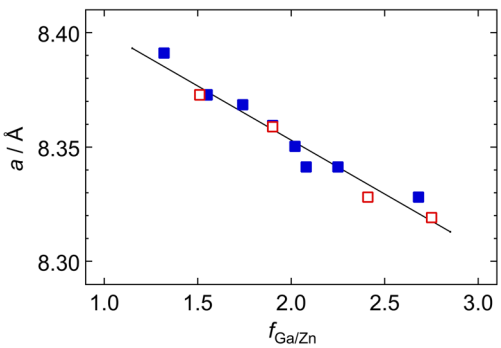

Fig. 6 Lattice parameter, a, for the spinel structure of the ZGO particles having various compositions ($f_{Ga/Zn}$), where each value of a is estimated from the diffraction angle for the (311) reflection in the XRD pattern: □ C_{cit} = 0 mmol L^{-1} and ■ C_{cit} = 40 mmol L^{-1}.

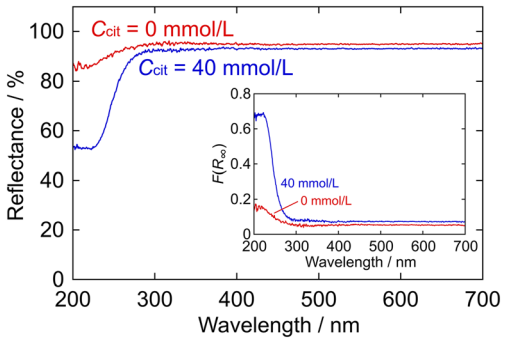

Fig. 7 Diffuse reflectance spectra and the respective Kubelka–Munk function $F(R_\infty)$ (the inset) of the present ZGO particles dispersed in a $BaSO_4$ matrix at 1 wt%. The red lines correspond to the sample prepared in the absence of Na_3-Cit (D = 9.5 nm and $f_{Ga/Zn}$ = 1.90), and the blue lines correspond to the sample prepared in the presence of Na_3-Cit at C_{cit} = 40 mmol L^{-1} (D = 138 nm and $f_{Ga/Zn}$ = 1.90).

the ionic radius of Ga^{3+} is smaller than that of Zn^{2+}, *i.e.*, 0.61 Å and 0.74 Å for 4-coordinate Ga^{3+} and Zn^{2+} ions; 0.76 Å and 0.88 Å for 6-coordinate Ga^{3+} and Zn^{2+} ions, respectively.[54]

Band gap estimation from the diffuse reflectance spectra

Fig. 7 shows the diffuse reflectance spectra of the ZGO particles (D = 9.5 nm and $f_{Ga/Zn}$ = 1.90 for C_{cit} = 0 mmol L^{-1}; D = 138 nm and $f_{Ga/Zn}$ = 1.90 for 40 mmol L^{-1}). The Kubelka–Munk function, $F(R_\infty)$, converted as follows:

$$F(R_\infty) = K/S = (1 - R_\infty)^2/2R_\infty \quad (4)$$

is also indicated in the inset, where K and S are the extinction and back-scattering coefficients, respectively; R_∞ is the absolute reflectance of the ZGO particles and is assumed to be equal to the measured reflectance. In accord with the white color of the ZGO powder, the reflectance in the visible region is constant for each sample, whereas the reflectance decreases at $\lambda \leq 300$ nm. The difference in reflectance and the $F(R_\infty)$ value would be due to the particle size difference (9.5 nm and 138 nm for C_{cit} = 0 mmol L^{-1} and 40 mmol L^{-1}, respectively).

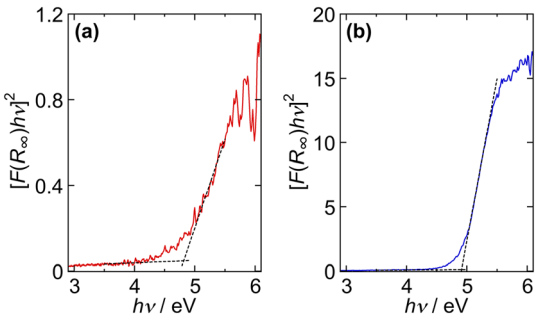

Fig. 8 Tauc plots for the ZGO particles using the $F(R_\infty)$ values in the inset of Fig. 7. The ZGO particles were prepared at (a) C_{cit} = 0 mmol L^{-1} ($f_{Ga/Zn}$ = 1.90 and D = 9.5 nm) and (b) C_{cit} = 40 mmol L^{-1} ($f_{Ga/Zn}$ = 1.90 and D = 138 nm).

To estimate the band gap energy, E_g, $[F(R_\infty)h\nu]^2$ is plotted as a function of $h\nu$ in Fig. 8 based on the Tauc relationship for the direct allowed transition, as follows:

$$(\alpha h\nu)^2 = A(h\nu - E_g), \quad (5)$$

where h is Planck's constant, ν is the frequency of the light, α is the absorption constant ($\propto F(R_\infty)$), and A is the proportional constant. The cross points of the extrapolated dotted lines give the E_g values of 4.81 eV and 4.91 eV for C_{cit} = 0 mmol L^{-1} (Fig. 8a) and 40 mmol L^{-1} (Fig. 8b), respectively. The E_g values appear reasonable given that they fall within the range of the reported values in the literature.[6,10] It should be noted that the E_g values are almost independent of $f_{Ga/Zn}$ under both C_{cit} conditions (E_g = 4.7–4.9 eV; see Fig. S7 in SI).

Fig. 9 shows the fluorescence spectra of the ZGO particles, where the wavelength range for the excitation spectra corresponds to the photon energy $E_p \geq 4.6$ eV. The excitation and emission peaks are located at 217 nm and 299 nm, respectively; the peak wavelengths are independent of the C_{cit} conditions, whereas the peak intensity is somewhat higher in the presence of Na_3-Cit, which is probably due to the size difference. Bluish-white light fluorescence was observed from each ZGO powder, reflecting the continuous emission spectrum in the visible region.

Among the present ZGO particles, there seems to be almost no difference in their optical properties, except for their diffuse reflectance. Their similar E_g values and FL spectra imply a consistent band structure, at least in the present particle size range (D = 10–200 nm).

Conclusions

The present study has successfully established a procedure for the synthesis of monodisperse zinc gallium oxide (ZGO) nanoparticles, enabling systematic control over their size and composition *via* the hydrothermal process, utilizing trisodium citrate as a complexing agent. The size of the ZGO

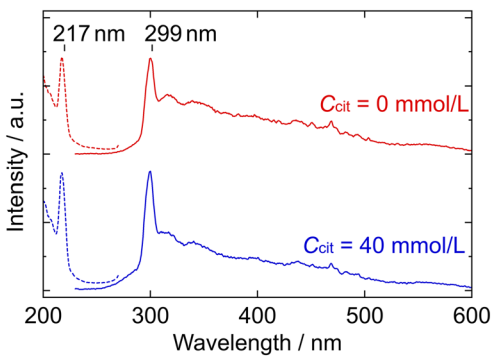

Fig. 9 Fluorescence spectra of the ZGO particles prepared at C_{cit} = 0 mmol L^{-1} ($f_{Ga/Zn}$ = 1.90 and D = 9.5 nm) and C_{cit} = 40 mmol L^{-1} ($f_{Ga/Zn}$ = 1.90 and D = 138 nm). The excitation spectra (broken lines) were measured by monitoring at 299 nm, whereas the emission spectra (solid lines) were recorded by irradiating at 217 nm.

particles is tuneable up to about 200 nm based on the citrate concentration, C_{cit}. The compositional ratio of Ga to Zn in the particles, $f_{Ga/Zn}$, depends on the Ga/Zn ratio in the reacting solution, C_{Ga}/C_{Zn}, and the C_{cit} level. At least in the range of $f_{Ga/Zn}$ = 1.3–2.7, all the prepared ZGO particles possess a spinel structure; however, their lattice parameter slightly decreased at a higher $f_{Ga/Zn}$. The absorption edges in the diffuse reflectance spectra indicate a band gap energy of E_g = 4.7–4.9 eV, which is almost independent of particle size and composition. The photoluminescence properties are also similar among the particle sizes, where their excitation and emission maxima are located at 217 nm and 299 nm, respectively. Due to the wide-range emission spectrum of the ZGO particles, they exhibit blueish-white light emission under a sufficiently short wavelength of UV light.

Author contributions

F. S. designed the study and prepared the manuscript. F. S. and N. K. synthesized and characterized the particles. All the authors discussed the results.

Conflicts of interest

There are no conflicts to declare.

Data availability

The data supporting this article have been included as part of the supplementary information (SI).

Supplementary information: HR-TEM image, TEM-EDX spectra, XRD pattern of the white precipitate, solubility estimations for the metal hydroxides, histograms of size for the ZGO particles, XRD peak shift by the ZGO composition, and Tauc's plots for the ZGO particles of different composition are available. See DOI: https://doi.org/10.1039/d5ce00952a.

Acknowledgements

The XRD patterns were obtained at the Center for Analytical Instrumentation, Chiba University.

Notes and references

1 T. Sugimoto, *Monodisperse Particles*, Elsevier, Amsterdam, 2nd edn, 2019.
2 V. K. LaMer and R. H. Dinegare, *J. Am. Chem. Soc.*, 1950, **72**, 4847.
3 J. Hornstra and E. Keulen, *Philips Res. Rep.*, 1972, **27**, 76.
4 M. Allix, S. Chenu, E. Veŕon, T. Poumeyrol, E. A. Kouadri-Boudjelthia and F. Fayon, *Chem. Mater.*, 2013, **25**, 1600.
5 M. Hirano, M. Imai and M. Inagaki, *J. Am. Ceram. Soc.*, 2000, **83**, 977.
6 E. Chikoidze, C. Sartel, I. Madaci, H. Mohamed, C. Vilar, B. Ballesteros, F. Belarre, E. del Corro, P. Vales-Castro, G. Sauthier, L. Li, M. Jennings, V. Sallet, Y. Dumont and A. Peŕez-Tomaś, *Cryst. Growth Des.*, 2020, **20**, 2535.
7 J. Xue, S. Wu and J. Li, *J. Am. Ceram. Soc.*, 2013, **96**, 2481.
8 Y. Teng, L. X. Song, W. Liu, Z. Y. Xu, Q. S. Wang and M. M. Ruan, *J. Mater. Chem. C*, 2016, **4**, 3113.
9 P.-H. Huang, Y.-C. Shen, C.-Y. Tung, C.-Y. Huang, C. S. Tan and R.-H. Horng, *ACS Appl. Electron. Mater.*, 2020, **2**, 3515.
10 A. K. Singh, C.-C. Yen, S.-M. Huang, C.-Y. Huang, H.-Y. Chou and D.-S. Wuu, *ACS Appl. Electron. Mater.*, 2024, **6**, 1356.
11 H. S. Roh, Y. C. Kang, S. B. Park and H. D. Park, *Jpn. J. Appl. Phys.*, 2002, **41**, 4559.
12 J. S. Kim, S. G. Lee, H. L. Park, J. Y. Park and S. D. Han, *Mater. Lett.*, 2004, **58**, 1354.
13 T. Dazai, S. Yasui, T. Taniyama and M. Itoh, *Inorg. Chem.*, 2020, **59**, 8744.
14 T. A. Safeera and E. I. Anila, *Scr. Mater.*, 2018, **143**, 94.
15 N. D. Hebbar, K. S. Choudhari, N. Pathak, S. A. Shivashankar and S. D. Kulkarni, *New J. Chem.*, 2022, **46**, 7032.
16 A. Bessière, S. K. Sharma, N. Basavaraju, K. R. Priolkar, L. Binet, B. Viana, A. J. J. Bos, T. Maldiney, C. Richard, D. Scherman and D. Gourier, *Chem. Mater.*, 2014, **26**, 1365.
17 T. Luan, J. Liu, X. Yuan and J.-G. Li, *Nanoscale Res. Lett.*, 2017, **12**, 219.
18 W. Fan, N. Lu, C. Xu, Y. Liu, J. Lin, S. Wang, Z. Shen, Z. Yang, J. Qu, T. Wang, S. Chen, P. Huang and X. Chen, *ACS Nano*, 2017, **11**, 5864.
19 E. Arroyo, B. Medrán, V. Castaing, G. Lozano, M. Ocaña and A. I. Becerro, *J. Mater. Chem. C*, 2021, **9**, 4474.
20 X. Wei, S. V. Kershaw, X. Huang, M. Jiao, C. C. Beh, C. Liu, M. Sarmadi, A. L. Rogach and L. Jing, *J. Phys. Chem. Lett.*, 2021, **12**, 7067.
21 B. B. Srivastava, S. K. Gupta and Y. Mao, *CrystEngComm*, 2020, **22**, 2491.
22 T. Maldiney, B.-T. Doan, D. Alloyeau, M. Bessodes, D. Scherman and C. Richard, *Adv. Funct. Mater.*, 2015, **25**, 331.
23 D. P. Dutta, R. Ghildiyal and A. K. Tyagi, *J. Phys. Chem. C*, 2009, **113**, 16954.
24 A. Tuerdi and A. Abdukayum, *RSC Adv.*, 2019, **9**, 17653.
25 B. B. Srivastava, S. K. Gupta and Y. Mao, *J. Mater. Chem. C*, 2020, **8**, 6370.
26 Y. Liu, T. Zheng, X. Zheng and C. Chen, *Sci. Rep.*, 2023, **13**, 14430.
27 C. Fang, S. Wang, S. Wei, Q. Xu, Z. Lyu, S. Shen, T. Tan and H. You, *Dalton Trans.*, 2024, **53**, 6377.
28 N. Kumagai, L. Ni and H. Irie, *Chem. Commun.*, 2011, **47**, 1884.
29 T. Zheng, Y. Xia, X. Jiao, T. Wang and D. Chen, *Nanoscale*, 2017, **9**, 3206.
30 Q. Liu, D. Wu, Y. Zhou, H. Su, R. Wang, C. Zhang, S. Yan, M. Xiao and Z. Zou, *ACS Appl. Mater. Interfaces*, 2014, **6**, 2356.
31 Y. Zhang, P. Li, L.-Q. Tang, Y.-Q. Li, Y. Zhou, J.-M. Liu and Z.-G. Zo, *Dalton Trans.*, 2017, **46**, 10564.
32 M. Takemoto, Y. Tokudome, K. Teramura, T. Tanaka, A. Nakahira and M. Takahashi, *RSC Adv.*, 2020, **10**, 8066.

33 X. Chen, H. Xue, Z. Li, L. Wu, X. Wang and X. Fu, *J. Phys. Chem. C*, 2008, **112**, 20393.
34 M. Sun, D. Li, W. Zhang, Z. Chen, H. Huang, W. Li, Y. He and X. Fu, *J. Solid State Chem.*, 2012, **190**, 135.
35 L. Liu, J. Huang, L. Cao, J. Wu, J. Fei, H. Ouyang, F. Ma and C. Zhou, *Mater. Lett.*, 2013, **95**, 160.
36 X. Li, X. Zhang, X. Zheng, Y. Shao, M. He, P. Wang, X. Fu and D. Li, *J. Mater. Chem. A*, 2014, **2**, 15796.
37 J. Li, W. Lu, H. Wu, L. Jin, B. Hu, L. Li and Z. Wang, *Mater. Sci. Semicond. Process.*, 2016, **56**, 251.
38 S. Y. Bae, H. W. Seo, C. W. Na and J. Park, *Chem. Commun.*, 2004, 1834.
39 A. R. Phani, S. Santucci, S. Di Nardo, L. Lozzi, M. Passacantando and P. Picozzi, *J. Mater. Sci.*, 1998, **33**, 3969.
40 L. Zou, X. Xiang, M. Wei, F. Li and G. Evans, *Inorg. Chem.*, 2008, **47**, 1361.
41 X. L. Duan, D. R. Yuan, L. H. Wang, F. P. Yu, X. F. Cheng, Z. Q. Liu and S. S. Yan, *J. Cryst. Growth*, 2006, **296**, 234.
42 M. Hirano, *J. Mater. Chem.*, 2000, **10**, 469.
43 M. Hirano and N. Sakaida, *J. Am. Ceram. Soc.*, 2002, **85**, 1145.
44 F. Conrad, Y. Zhou, M. Yulikov, K. Hametner, S. Weyeneth, G. Jeschke, D. Günther, J.-D. Grunwaldt and G. R. Patzke, *Eur. J. Inorg. Chem.*, 2010, 2036.
45 M. Hirano and N. Sakaida, *J. Ceram. Soc. Jpn.*, 2003, **111**, 0176.
46 W. Yang, J. Li, X. Zhang, C. Zhang, X. Jiang and B. Liu, *Inorg. Chem.*, 2019, **58**, 549.
47 K. Fuda, N. Kudo, S. Kawai and T. Matsunaga, *Chem. Lett.*, 1993, 777.
48 R. Von Allmann, *Chimia*, 1970, **24**, 99.
49 Y. Zhang, H. Xu and S. Lu, *RSC Adv.*, 2021, **11**, 24254.
50 Y. F. Orlov and E. I. Belkina, *Russ. J. Inorg. Chem.*, 2011, **56**, 975.
51 N. C. Li, A. Lindenbaum and J. M. White, *J. Inorg. Nucl. Chem.*, 1959, **12**, 122.
52 W. R. Harris and A. E. Martell, *Inorg. Chem.*, 1976, **15**, 713.
53 T. Sugimoto, F. Shiba, T. Sekiguchi and H. Itoh, *Colloids Surf., A*, 2000, **164**, 183.
54 F. A. Cotton, G. Wilkinson, C. A. Murillo and M. Bochmann, *Advanced Inorganic Chemistry*, Wiley, New York, 6th edn, 1999, p. 1303.

